International Journal of Concrete Structures and Materials

RESEARCH

Open Access

Enhancing the Flexural Capacity of Deteriorated Low-Strength Prestressed Concrete Beam Using Near-Surface Mounted Post-Tensioned Carbon Fiber-Reinforced Polymer Bar

Sanghyeon Cho[1], Wonseok Chung[1*], Woo-tai Jung[2], Jong-sup Park[2] and Heeyoung Lee[3*]

Abstract

This study aimed to address the critical issue of age deterioration in prestressed concrete (PSC) structures by investigating the strengthening of aged PSC structures using a near-surface mounted (NSM) post-tensioned carbon fiber-reinforced polymer (CFRP). A total of nine PSC beams, each with a length of 6.5 m, were fabricated for a four-point bending test. Various experimental parameters were taken into account, including the strengthening method, compressive strength of concrete in the PSC beam, and the prestressing force of the PSC beam. The results indicated that the NSM post-tensioned CFRP strengthening system proved more efficient when compared to the NSM non-post-tensioned CFRP strengthening system. The flexural capacity of the NSM post-tensioned CFRP strengthening system, under the deteriorated low-strength PSC beam, increased by up to 30.9% compared to the PSC reference beam. Additionally, the experimental results were compared to a finite-element analysis, and a parametric study was conducted to examine the material properties of the PSC beam. Consequently, the NSM post-tensioned CFRP strengthening system is expected to be an effective solution for addressing the issue of deteriorated low-strength PSC structures.

Keywords PSC, Near-surface mounted, Post-tensioned CFRP, Flexural capacity, Finite-element analysis

1 Introduction

Over 50% of the concrete bridges constructed in North America since 1997 have been constructed using prestressed concrete (PSC) (Collins & Mitchell, 1997). According to the ASCE 2021 report for America infrastructure (Hermann, 2013), 42% of all concrete bridges in USA are over 50 years old, 7.5% of which are structurally deficient. Therefore, it has become necessary to limit deterioration in PSC structures. The flexural capacity of PSC structures decreases owing to long-term exposure to the external environment. In other words, the long-term use of deicing salts or construction in coastal zones increases the failure probability of concrete structures by up to 50 times owing to the influence of chloride ions (Stewart & Rosowsky, 1998). In Xaing and Zhao

Journal information: ISSN 1976-0485 / eISSN 2234-1315.

*Correspondence:
Wonseok Chung
wschung@khu.ac.kr
Heeyoung Lee
heeyoung0908@chosun.ac.kr
[1] Department of Civil Engineering, Kyung Hee University, 1732 Deokyoung-Daero, Giheung-Gu, Yongin-Si, Gyeonggi-Do 17104, South Korea
[2] Advanced Composites Research Center, Korea Institute of Civil Engineering and Building Technology, 283, Goyang-Daero, Ilsanseo-Gu, Goyang-Si, Gyeonggi-Do 10223, South Korea
[3] Department of Civil Engineering, Chosun University, 309 Pilmun-Daero, Dong-Gu, Gwangju 61452, South Korea

(2007), the compressive strength decreased depending on chloride ion penetration. Yildirim and Sümer (2013) demonstrated that the compressive strength cured in chloride solution for 90 days was 40% lower than that cured in normal water. Wongkeo et al. (2014) conducted a study using chloride ions and stated that the compressive strength decreased by 48% compared to the reference specimen after curing for 90 days. Zhao et al. (2020) placed a concrete specimen in chloride solution and cured it for 12 months. As experimental results, the compressive strength of the concrete decreased by 20% compared to the maximum compressive strength of the reference specimen. Caro et al. (2013) found that when the anchorage of the PSC structure is realized and maintained for a year, the prestress loss could be up to 60% of the maximum total prestress. Asamoto et al. (2014) reported that the prestress loss can be reduced to 30% of the maximum value by burying a steel strand in the concrete, introducing prestress, and maintaining the system for 127 days. Páez and Sensale (2018) was found to show 22% prestress loss after 6.5 years at PSC beam. Pisani (2018) predicted behavior of a prestressed box girder with a length of 4 m. As a result, the prestress loss can occur more than 20% after about 137 years. You and Kaewunruen (2019) observed a 24% prestress loss after introducing prestress into a 2.6 m-long concrete sleeper and maintaining the prestress for 2 years. Ye et al. (2020) analyzed the behavior of an 11.9 m-long PSC girder for 897 days and observed a prestress loss of up to 16%. The compressive strength of structures constructed using PSC decreases owing to long exposure to the external environment after construction, resulting in prestress loss and a decrease in flexural capacity. Therefore, deteriorated PSC structures require improved flexural capacity to reduce the prestress loss and aging of concrete. Vollmer et al. (2021) conducted a steel material experiment and found that the prestress loss can be occurred by at least 25% when a general steel strand is used over 2 years.

Recently, the external prestressing system was investigated as a reinforcement method, wherein a prestressed steel bar was installed on the exterior wall of the PSC structure (Allawi, 2017; Kim et al., 2021; Kwon et al., 2018). However, considering the steel bar is exposed to the outside environment, it could lead to accelerated corrosion. The near-surface mounted (NSM) strengthening system was suggested as an alternative to the external prestressing system considering it can protect the reinforcement under poor conditions by embedding reinforcement on the concrete surface. Recently, research was conducted to increase the flexural capacity of the NSM strengthening system and its resistance to the external environment by replacing steel bars with fiber-reinforced polymer (FRP) materials. Among the different FRP materials, carbon FRP (CFRP) possesses a high corrosion and fatigue resistance and high strength. The standards for the NSM FRP strengthening system have been proposed by the USA, Canada, and Japan (American Concrete Institute, 2015; Canadian Standards Association, 2021; Japan Society of Civil Engineers, 2007). The NSM FRP strengthening systems have improved in terms of flexural, shearing, and bonding behavior over the past decade (Seo et al., 2016; Hong et al., 2018; Jafari et al., 2018; Noroozieh & Mansouri, 2019; Barham et al., 2021; Salman & Mansor, 2021; Panahi et al., 2021; Mansour & El-Maaddawy, 2021; Haddad & Yaghmour, 2020; Yu et al., 2020; Ahmed et al., 2023).

Compared to a general external prestressing system, NSM FRP strengthening system that uses non-post-tensioned FRP bars has a smaller strengthening effect owing to the absence of prestressing. Therefore, the NSM post-tensioned FRP strengthening system was developed by introducing prestressing to FRP. These studies investigated the ideal length and properties of FRP and analyzed reinforced concrete (RC) beams with a length of 3.3–4.0 m (Badawi & Soudki, 2009; Esmaeeli & He, 2021; Nordin & Täljsten, 2006). Results showed that the flexural capacity increased by 15–97% after a prestressed FRP bar was introduced. Peng et al. (2014) classified 3.5 m-long RC beams into NSM FRP strengthening system, externally bonded FRP strengthening system, and NSM post-tensioned FRP strengthening system, and evaluated them. In the NSM post-tensioned FRP strengthening system, the ultimate load increased by up to 44% compared to the NSM non-post-tensioned FRP strengthening system and external bonded FRP strengthening system. Correia et al. (2015) analyzed the flexural behavior of a 2.6 m-long RC slab according to the NSM post-tensioned FRP strip strengthening system. The ultimate strength of the strengthened slab with the NSM post-tensioned FRP strengthening system improved by up to 1.7 times compared to the RC reference slab. Hong and Park (2016) analyzed the flexural capacity of the NSM post-tensioned FRP strengthening system under RC beam. Compared to the RC reference beam, the ultimate load of the strengthened RC beam increased by 96%. In Kara et al. (2016), when the prestressing force increased to 60% of the ultimate load of the CFRP bar, the ultimate moment increased. Wu et al. (2014) analyzed a 2 m-long RC beam whose behavior changed according to the number of FRPs and type of FRP end. When the optimum NSM post-tensioned FRP strengthening system was fabricated, the ultimate load increased by up to 71% compared to the RC reference beam. Lee et al. (2017a) applied the NSM post-tensioned FRP strengthening system to RC beam with a 6.4 m long and analyzed the

NSM post-tensioned CFRP strengthening system using the prestressing method of the CFRP bar. Results showed that the post-tension method was superior to the pre-tension method. Compared with a fully bonded system, Choi et al. (2011) reported a 14% decrease in the ultimate load in their partially unbonded system as the unbound length section increased in the NSM post-tensioned FRP strengthening system. Lee et al. (2019) fabricated an RC beam and analyzed the flexural behavior of the NSM post-tensioned FRP strengthening system based on the bonded/unbonded criterion, compressive strength, and the degree of damage. El-Hacha and Gaafar (2011) analyzed the failure behavior of RC beam according to the prestressing force and prestress losses. The strengthened RC beam with the NSM post-tensioned FRP strengthening system was found to be most effective when the prestressing force was 40% of the ultimate strength of the CFRP bar. Lee et al. (2018) applied the NSM post-tensioned FRP strengthening system to an old RC bridge and analyzed flexural behavior. Results showed that the displacement decreased by 31% compared to the reference bridge, indicating improved on-site applicability. Sokairge et al. (2022) applied the NSM post-tensioned FRP strengthening system to the RC beam with a length of 3.3 m, and the ultimate load increased 1.4 times compared to the RC reference beam. Cho et al. (2022) analyzed the strengthening of the NSM post-tensioned CFRP strengthening system based on the degree of deterioration in the RC beams. The parameters of the test were the compressive strength of concrete, steel reinforcement ratio, and the number of CFRP bars. The ultimate load of the strengthened RC beam with the NSM post-tensioned CFRP strengthening system improved by up to 106.5% compared to the reference beam. The NSM post-tensioned CFRP strengthening system had an excellent strengthening effect on the deteriorated RC beams. Lee et al. (2017b) used a 21.8 m-long full-scale PSC girder and analyzed the strengthening effect based on the introduction of the NSM post-tensioned CFRP strengthening system. Results showed that as the number of CFRP bars and pressing load increased, the ultimate load increased by up to 13% compared to the PSC reference girder.

Most studies conducted on NSM post-tensioned FRP strengthening systems (Badawi & Soudki, 2009; Correia et al., 2015; Esmaeeli & He, 2021; Hong & Park, 2016; kara et al., 2016; Lee et al., 2017a, 2017b; Nordin & Täljsten, 2006; Peng et al., 2014; Wu et al., 2014(a); Choi et al., 2011; Lee et al., 2019; El-hacha & Gaafar, 2011; Lee et al., 2018; Sokairgeet al., 2022) analyzed the effects of introducing the NSM post-tensioned FRP strengthening system to an RC structure based on the flexural capacity. Cho et al. (2022) analyzed the flexural behavior of the strengthened RC structure with the NSM post-tensioned CFRP strengthening system according to the degree of deterioration; however, they did not analyze the NSM post-tensioned CFRP strengthening system under PSC structure. Furthermore, Lee et al. (2017b) only focused on the flexural capacity of the full-scale PSC girder based on the introduction of the NSM post-tensioned CFRP strengthening system. The flexural capacity of PSC structures can deteriorate significantly owing to the aging concrete and corresponding prestress loss. Currently, approximately 50% of PSC structures are aging and require additional reinforcement. Furthermore, no studies have attempted reinforcing deteriorated PSC structures by applying a NSM post-tensioned CFRP strengthening system. Since the NSM post-tensioned CFRP strengthening system is effective in strengthening general deteriorated concrete structures, it is necessary to analyze whether this system has an excellent strengthening effect on deteriorated PSC structures. Therefore, this study analyzes the strengthening effect of the NSM post-tensioned CFRP strengthening system based on the degree of deterioration in a PSC structure by considering their flexural capacity and the different material properties of PSC beams. The PSC structure was implemented using a PSC beam. Strengthening methods were classified depending on the use of non-post-tensioned or post-tensioned CFRP bars, and the strengthening effect of each method was analyzed. Owing to the difficulties in implementing the deterioration of concrete and steel strands in the experiment, the deterioration was replaced using the compressive strength of concrete and prestressing force. Additionally, to investigate the deterioration, the compressive strength was set to 20 MPa (deteriorated concrete) and 40 MPa (normal concrete) (Herrmann, 2021; Xaing and Zhao, 2007; Yildirim & Sümer, 2013; Wongkeo et al., 2014; Zhao et al., 2020). For the steel strand, an appropriate prestressing force (280 kN) was applied by referring to the standard (American Concrete Institute, 2019). In previous studies (Caro et al., 2013; Asamoto et al., 2014; Páez and Sensalem, 2018; Pisani, 2018; You & Kaewunruen, 2019; Ye et al., 2020; Vollmer et al., 2021), a prestress loss between 15 and 60% was observed; therefore, in this study, the prestressing force of the steel strand was classified using the appropriate prestressing force (280 kN) and half its value (140 kN) to evaluate the prestress loss. Furthermore, this study aims to analyze the difference ratio of the design compared to test by comparing the design strength and the experimental results of a PSC beam strengthened by the NSM post-tensioned CFRP strengthening system. Finite-element analysis (FEA) was conducted to forecast the flexural behavior of the NSM post-tensioned CFRP strengthening system under PSC beam according to the different compressive strengths of concrete and the steel

reinforcements. Finally, the suggested finite-element (FE) model is compared with the test unit in a parametric study.

2 Design of NSM Post-Tensioned CFRP Strengthening System

The NSM post-tensioned CFRP strengthening system uses the same mechanism as the prestressing system of general PSC structures. Considering this, Cho et al. (2022) referred to the design process of the prestressing system (American Concrete Institute, 1999) and predicted the experimental results within a slight error. In this study, the design process of the NSM post-tensioned CFRP strengthening system on the PSC and RC structures was similar. Therefore, the design process of the NSM post-tensioned CFRP strengthening system in Cho et al. (2022) was referred to.

The design process was performed in four steps. First, the compressive strain of the concrete and depth of the neutral axis is randomly assumed. Second, the strain of the CFRP bar is calculated based on the above assumptions. The calculation procedure to calculate the strain of the CFRP bar is presented in Cho et al. (2022). The compressive strain generated by the effective prestress introduced to the CFRP bar is calculated as

$$\varepsilon_1 = \frac{P_{frp}}{E_{frp}A_{frp}}, \tag{1}$$

where ε_1 and ε_2 are the effective strain by the effective prestress of the CFRP bar (P_{frp}) and the strain of the CFRP bar when the concrete stress at the neutral axis is 0, respectively. E_{frp} and A_{frp} are the elasticity and area of the CFRP bar, respectively. e_{frp} is the distance between the cross-section center of the PSC structure and the center of the CFRP bar. E_c and A_c are the elasticity and the area of concrete, respectively. r_c is the rotational radius. ε_3 is the strain of the CFRP bar that occurs when loading the ultimate load, d_{frp} is the effective depth of the CFRP bar, c is the neutral axis of the cross-section, and ε_{frp} is the total strain of the post-tensioned CFRP bar ($\varepsilon_1 + \varepsilon_2 + \varepsilon_3$).

In the PSC structure, the stress concentrated at the position where the prestressing force of the CFRP bar is introduced is distributed throughout the PSC structure over time. After completing the stress redistribution of the PSC structure, the concrete stress becomes 0 at the neutral axis, and the strain of the CFRP bar is as follows

$$\varepsilon_2 = \frac{P_{frp}}{E_cA_c}\left(1 + \frac{e_{frp}^2}{r_c^2}\right). \tag{2}$$

Subsequently, the strain of the CFRP bar, until it reaches the ultimate load, is calculated as

$$\varepsilon_3 = \varepsilon_{cu}\frac{d_{frp} - c}{c}. \tag{3}$$

The total strain of the post-tensioned CFRP bar (ε_{frp}) is obtained from the sum of ε_1, ε_2, and ε_3.

Third, the tensile force generated in the PSC structure was estimated using the NSM post-tensioned CFRP strengthening system. Finally, the equilibrium in the PSC structure were verified as

$$A_s'f_s' + 0.85f_{ck}\beta_1 cb = A_sf_s + A_{strand}E_{strand}\varepsilon_{strand} + A_{frp}E_{frp}\varepsilon_{frp}, . \tag{4}$$

where A_s' and f_s' are the cross-sectional area and compressive stress of the compressed steel reinforcement. f_{ck} is the compressive strength of the concrete, $\beta_1 c$ is the average stress depth, and b is the width of the concrete structure. A_s are the area of the tensile steel reinforcement, and f_s are the stress of the tensile steel reinforcement. A_{strand}, E_{strand}, and ε_{strand} are the area, elasticity, and strain of the steel strand, respectively.

Fig. 1 shows an example of the process of calculating the equilibrium between the compressive and tensile forces by repeating the above-mentioned steps. Under the first, the tensile and compressive forces are evaluated by setting random values to the compressive strain of the concrete and the depth of the neutral axis. Subsequently, the compressive strain and neutral axis depth were gradually adjusted to match the equilibrium. If the force is not balanced, the four-step process is repeated until equilibrium is obtained. Next, the initial bending moment at the initial crack and the maximum bending moment were calculated to predict the strength of the specimen. The bending moment at the initial crack in the PSC beam was calculated as

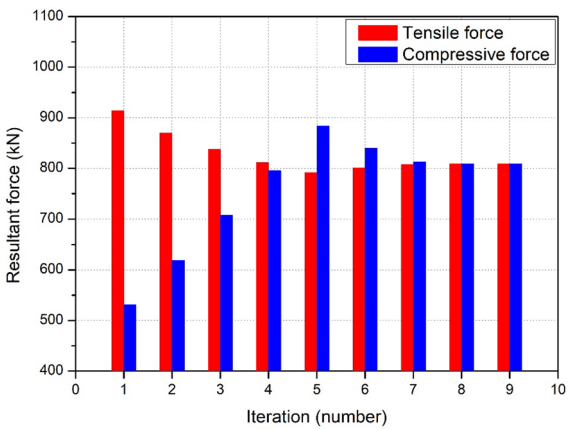

Fig. 1 Verification of the equilibrium of the compressive and tensile forces

$$M_{cr,d} = f_r \frac{I_c}{y_b} + P_{strand}\left(\frac{r_c^2}{y_b} + e_{strand}\right) + P_{frp}\left(\frac{r_c^2}{y_b} + e_{frp}\right), \tag{5}$$

where $M_{cr,d}$ and M_d are the initial bending moment and the maximum bending moment, respectively. f_r is the tensile strength of the concrete, P_{strand} is the effective stress introduced to the steel strand, e_{strand} is the distance from the cross-section center of the PSC structure to the center of the steel strand, I_c is the second moment of the concrete cross-section, and y_b is the distance of the cross-section to the center axis. d, d′, d_{strand}, and d_{frp} are the effective depths of the tensile steel reinforcement, compressive steel reinforcement, steel strand, and CFRP bar, respectively.

The equation used to calculate the initial crack load in the external prestressing system was employed. The maximum bending moment of the structure to which the NSM post-tensioned CFRP strengthening system was calculated as

$$\begin{aligned} M_d = {} & \left(A_s f_s - A_s' f_s'\right)\left(d - \frac{\beta_1 c}{2}\right) + A_s' f_s' (d - d') \\ & + A_{strand} E_{strand} \varepsilon_{strand}\left(d_{strand} - \frac{\beta_1 c}{2}\right) \\ & + A_{frp} E_{frp} \varepsilon_{frp} \left(d_{frp} - \frac{\beta_1 c}{2}\right). \end{aligned} \tag{6}$$

The design load was calculated after excluding the bending moment (M_s) from the maximum bending moment (M_d) by self-weight. The design load (P_d) was calculated using the bending moment and distance between the load and the boundary position (L), given as

$$\frac{P_d L}{2} = M_d - M_s. \tag{7}$$

The difference ratio of the design compared to experiment was calculated utilizing the load (P_t) and design load deduced from the experiments, given as

$$Difference\ ratio = \frac{P_t - P_d}{P_d} \times 100. \tag{8}$$

The design load at the initial crack and the maximum design load were estimated to predict the strength of the PSC structure to which the NSM post-tensioned CFRP strengthening system was introduced. The estimated values were then compared to the results obtained from the experiments to determine the difference ratio.

3 Experimental Method

A 6.5 m-long full-scale PSC beam with a height and width of 600 mm and 260 mm was fabricated, respectively. The surface of the CFRP bar was subjected to sand coating to improve its adhesion with epoxy. Fig. 2 shows the dimensions of the PSC beam and the NSM post-tensioned CFRP strengthening system.

Table 1 summarizes the experimental parameters, which were set according to the strengthening method, compressive strength of the concrete, and the prestressing force of the steel strand. A PSC reference beam with the strengthened PSC beam was fabricated for comparison. When naming the parameter, the first letters in name of the test unit denote the strengthening method: "NS" represents no strengthening, indicating the PSC reference beam, "NSM" represents the NSM without post-tensioned CFRP bar, and "PNSM" represents the NSM with post-tensioned CFRP bar. Both "NSM" and "PNSM" used one CFRP bar. The second letters denote the compressive strength of the concrete: "C20" and "C40" represent 20 MPa (deteriorated concrete) and 40 MPa (normal concrete), respectively. The third letter represents the prestressing force of the steel strand: "P140" and "P280" represent 140 kN and 280 kN, respectively. This study used two steel strands with a diameter of 12.7 mm and a cross-sectional area of 98.71 mm^2. The tensile strength of each steel strand is 183 kN.

The strengthened length with the CFRP bar was designed to be 4.92 m (76% of the total length of the PSC beam) (Lee et al., 2017b). The diameter of the CFRP bar was 10 mm, and the properties of the CFRP bar are summarized in Table 2. To prestress the concrete structures with CFRP, the prestressing force of the CFRP bar should be designed to be below 65% of the ultimate strength (American Concrete Institute, 2015). Therefore, 42% of the ultimate strength (240 kN), i.e., 100 kN, was loaded onto the CFRP bar, and the strain was 7,850 $\mu\varepsilon$.

Fig. 3 shows the manufacturing procedure of the test unit. The NSM post-tensioned CFRP strengthening system strengthened PSC beam was used to assemble the steel reinforcement (Fig. 3a). As shown in Fig. 3b, the mold of the test unit was fabricated, and the assembled steel reinforcement was installed inside the mold. The concretes were distinguished and poured into the mold according to their compressive strengths (Fig. 3b). Fig. 3c, d demonstrates the process of introducing prestress to the steel strand and forming the groove on the bottom surface of the PSC beam, respectively. For convenience purposes, the bottom surface of the PSC beam was positioned upward before creating the groove. After the groove was formed on the bottom surface, the anchorage device was installed at both ends of the CFRP bar and the bar was loaded, as shown in Fig. 3e. Fig. 3f demonstrates the process of injecting epoxy fillers into the groove to

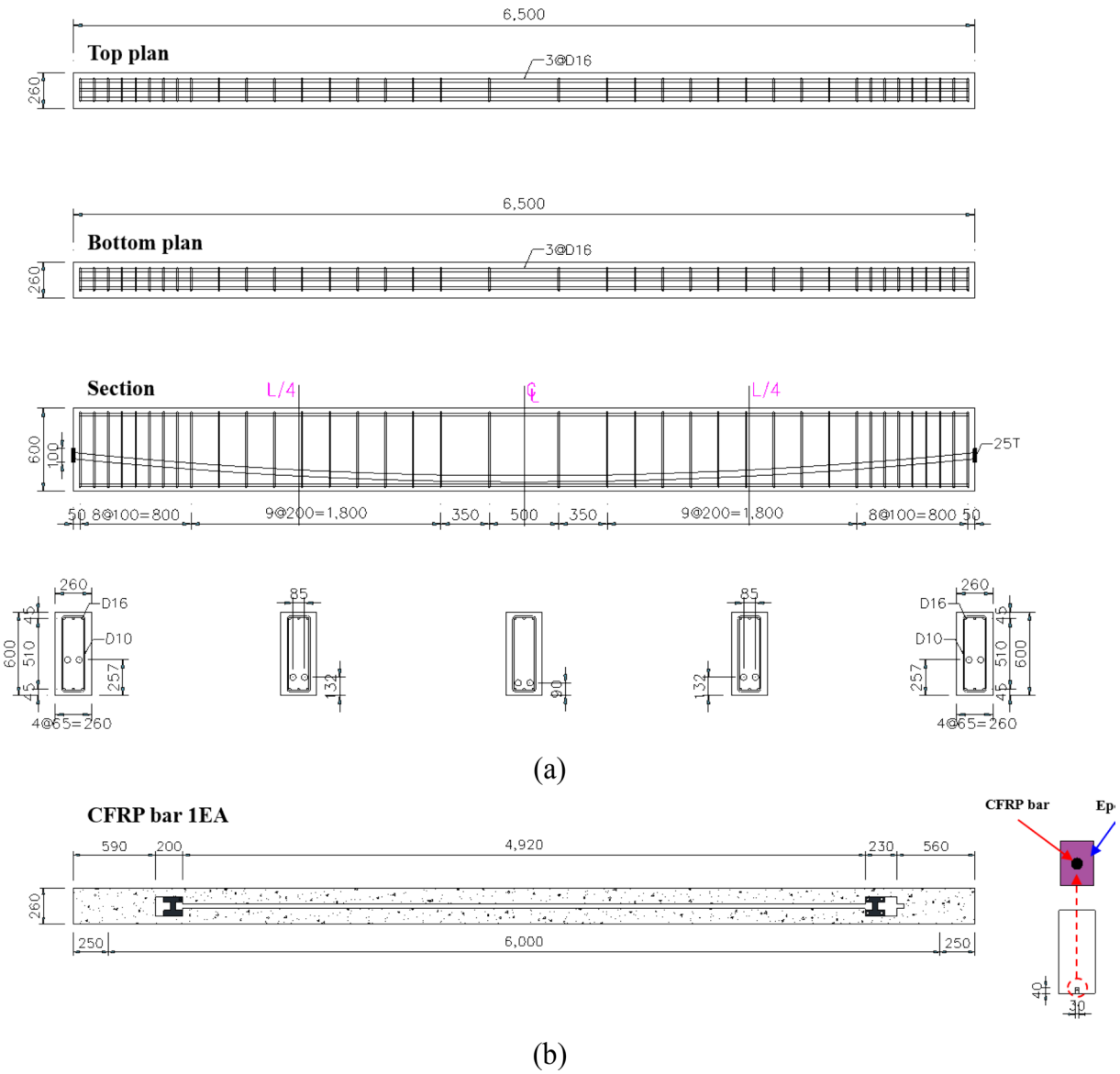

Fig. 2 Dimensions of (**a**) PSC beam and (**b**) NSM post-tensioned CFRP strengthening system (mm)

shield the NSM post-tensioned CFRP strengthening system. Herein, the concrete and epoxy were cured for over 28 days and 14 days, respectively, to implement sufficient strength. Since NSM post-tensioned CFRP strengthening system is mainly applied to the bottom of the bridge, epoxy is often injected upward. However, in this study, epoxy was injected as shown in Fig. 3 to idealize the condition.

Fig. 4 shows the four-point bending test. A universal testing machine (UTM) with a capacity of 2,000 kN was used for incremental static loading. The loading point was located 500 mm from the central axis on both sides of the PSC beam. The displacement was measured using the linear variable displacement transducer (LVDT) installed at the center of the PSC beam. The strain gauge on the CFRP bar was installed as shown in Fig. 4a to evaluate the test unit behavior. The vertical displacement rate was maintained at 0.03 mm/s for up to 30 mm, such that the initial crack could be visually identified. After the vertical displacement exceeded 30 mm, the vertical displacement rate was 0.1 mm/s. The boundary conditions of the PSC beam were set to a simple support, as shown in Fig. 4b.

Table 1 Experimental parameters

Test unit	Strengthening method	Compressive strength of the concrete (MPa)	Prestressing load of the steel strand (kN)
NS-C20-P140	No strengthening (NS)	20 (C20)	140 (P140)
NS-C20-P280			280 (P280)
NS-C40-P140		40 (C40)	140 (P140)
NS-C40-P280			280 (P280)
NSM-C20-P140	NSM non-post-tensioned CFRP strengthening system (NSM)	20 (C20)	140 (P140)
PNSM-C20-P140	NSM post-tensioned CFRP strengthening system (PNSM)	20 (C20)	140 (P140)
PNSM-C20-P280			280 (P280)
PNSM-C40-P140		40 (C40)	140 (P140)
PNSM-C40-P280			280 (P280)

Table 2 Properties of the CFRP bar

Ultimate strength (kN)	Tensile strength (MPa)	Ultimate strain ($\mu\varepsilon$)	Elastic modulus (MPa)
240	3,056	18,680	163,500

4 Experimental Results

Table 3 compares the design and experimental loads. The difference ratio of the design compared to experimental loads in the NSM post-tensioned CFRP strengthening system decreased as the compressive strength of the concrete increased. In 20 MPa of the compressive strength, difference ratios of up to 25.5% at the initial crack and 12.8% at the ultimate load were observed. When the compressive strength was 40 MPa, both difference ratios were below 3%. When the prestress was loaded onto the CFRP bar, the anchorage device for the PSC beam with low compressive strength was damaged at the point where the CFRP bar was fixed, which resulted in an increase in the difference ratio. Conversely, the PSC beam with a high compressive strength was not damaged in the peripheral concrete that fixes the anchorage device. This indicated that the experimental results were similar to the design strength.

Fig. 5 shows the displacement and strain results with and without prestressing load in the CFRP bar, and Table 4 summarizes the strengthening ratio between the strengthened PSC beam and PSC reference beam. In Fig. 5a, the initial concrete crack and steel yield loads of PNSM-C20-P140 were 44.8% and 19.1% higher than those of NS-C20-P140, respectively. The ultimate load of PNSM-C20-P140 was 278.0 kN, which was 22.1% higher than that of NS-C20-P140 (227.6 kN). The initial crack and steel yield loads of NSM-C20-P140 were 8.6% lower and 4.1% higher than that of NS-C20-P140, respectively. The ultimate load of NSM-C20-140 was 248.0 kN, which was 9.0% higher than that of NS-C20-P140. The strain in the CFRP bar under different loads is shown in Fig. 5b. The CFRP bar of PNSM-C20-P140 exhibited a strain of 7,850 $\mu\varepsilon$ under the prestressing force (100 kN). The strains of the CFRP bar of NSM-C20-P140 and PNSM-C20-P140 were 10,695 $\mu\varepsilon$ and 15,073 $\mu\varepsilon$, respectively, under the ultimate load. As a result, the flexural capacity of NSM-C20-P140, to which the prestressing force was not introduced, increased compared to the PSC reference beam (NS-C20-P140). The flexural strengthening effect of PNSM-C20-P140 was superior to that of NSM-C20-P140 owing to the introduction of the prestressing force. Furthermore, compared to the non-post-tensioned CFRP bar, the post-tensioned CFRP bar exhibited a higher strain at the same load level. The flexural strengthening effect of the CFRP bar increased with a higher strain at the same load level; therefore, PNSM-C20-P140, to which a prestressing force was applied, was an efficient flexural strengthening method.

Fig. 6 shows the load-displacement relationship under the compressive strength and prestressing force of the steel strand. Fig. 6a represents the case with a compressive strength of 20 MPa, while Fig. 6b represents the case with a compressive strength of 40 MPa. Table 5 summarizes the strengthening ratio between the strengthened PSC beam and PSC reference beam. PNSM-C20-P140, with a compressive strength of 20 MPa and prestressing force of 140 kN, exhibited a 44.8% higher initial crack load, 19.1% higher steel yield load, and 22.1% higher ultimate load compared to those of NS-C20-P140. PNSM-C20-P280, with a compressive strength of 20 MPa and prestressing force of 280 kN, exhibited an 11.4% higher initial crack load, 22.3% higher steel yield load, and

(a) Assembling the steel reinforcement

(b) Assembling the mold and pouring the concrete

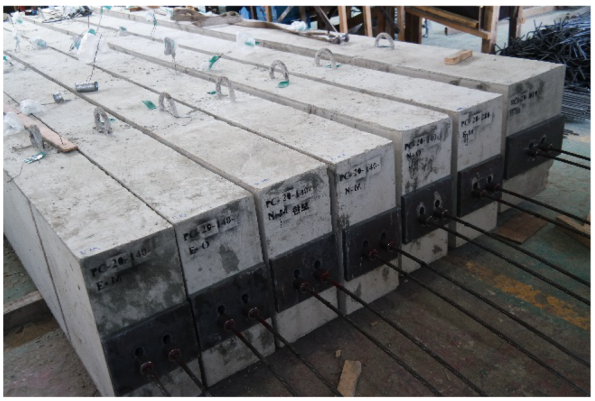

(c) Prestressing the steel strand

(d) Forming the groove upside down

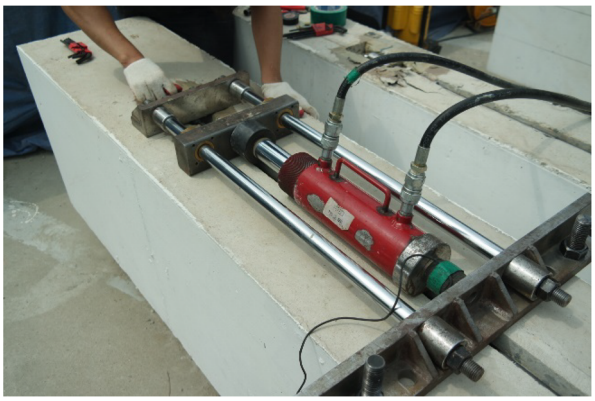

(e) Placing anchor and prestressing the CFRP bars

(f) Injecting filler in the groove

Fig. 3 Fabrication process of the test unit

24.4% higher ultimate load compared to those of NS-C20-P280. PNSM-C40-P140, with a 40 MPa compressive strength and 140 kN prestressing force, exhibited a 44.9% increase in the initial crack load compared to those of NS-C40-P140. The steel yield load of PNSM-C40-P140 was 23.1% higher than that of NS-C40-P140,

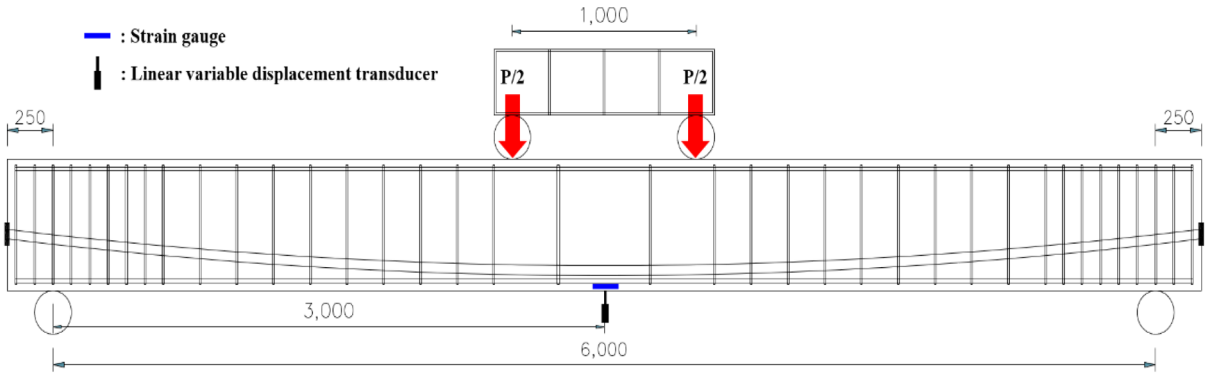

(a) Loading and sensor installation

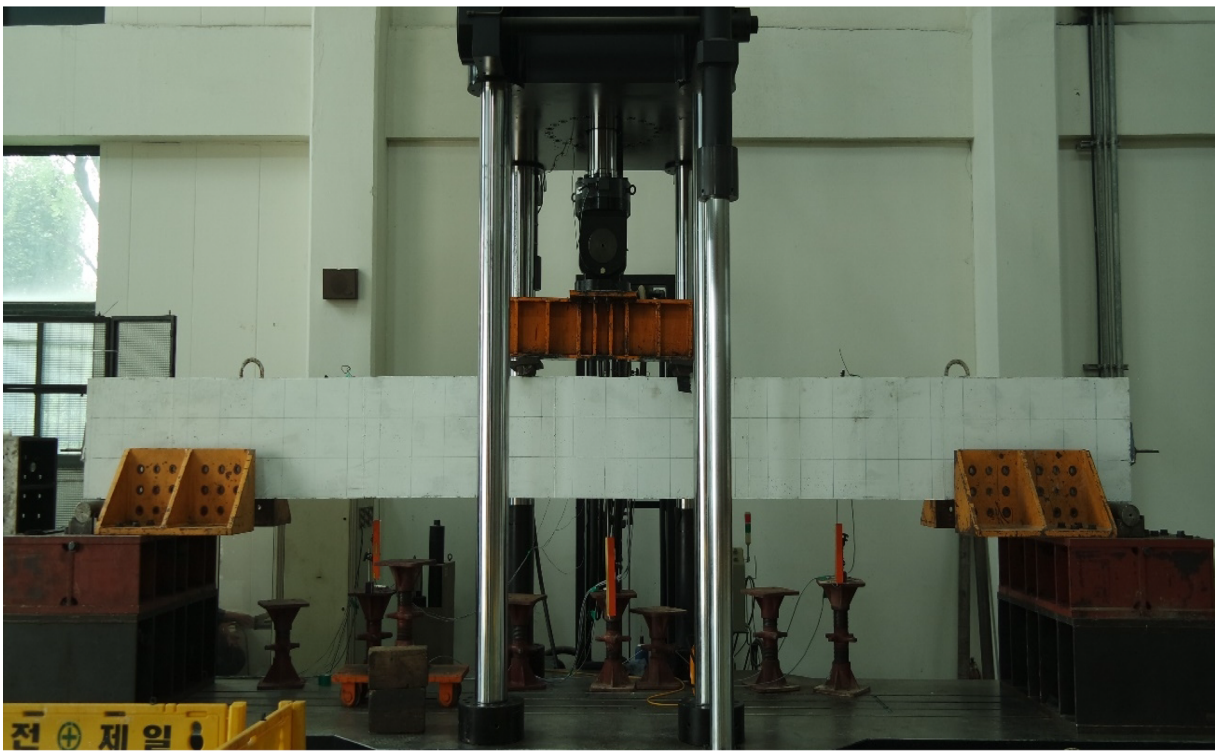

(b) Photograph of the experimental set-up

Fig. 4 Four-point bending test

Table 3 Comparison of the design load compared to experimental load

Test unit	P_{cr}(kN)		Difference ratio (%)	P_u(kN)		Difference ratio (%)
	Design	Experiment		Design	Experiment	
NS-C20-P140	57.2	42.6	−25.5	227.0	248.0	+9.3
PNSM-C20-P140	81.2	67.5	−16.9	256.0	278.0	+8.6
PNSM-C20-P280	113.3	86.3	−23.8	257.0	290.0	+12.8
PNSM-C40-P140	93.6	92.3	−1.4	303.0	300.0	−1.0
PNSM-C40-P280	125.7	122.6	−2.5	304.0	311.0	+2.3

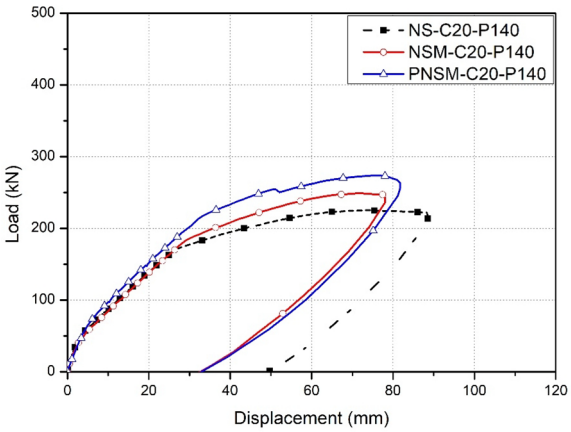

(a) Displacement

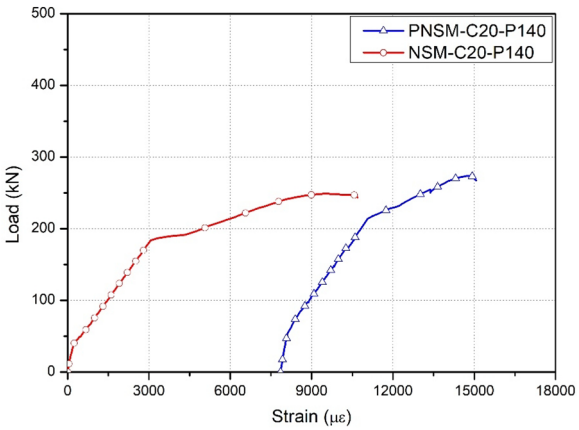

(b) Strain of the CFRP bar

Fig. 5 Displacement and strain results with and without prestressing in the CFRP bar

whereas the ultimate load increased by 25.4%. When the prestressing force was 280 kN (PNSM-C40-P280), the initial crack, steel yield, and ultimate load increased by 31.1%, 31.1%, and 30.9%, respectively, compared to NS-C40-P280. Under the initial crack load, the difference in the strengthening ratio between PNSM-C20-P140 and PNSM-C20-P280 was higher than 30%. Considering PNSM-C20-P140 had a relatively low amount of reinforcement attributed to the prestressing force of the steel strand, the strengthening effect owing to the NSM post-tensioned CFRP strengthening system was large. However, because PNSM-C20-P280 exhibited a higher amount of reinforcement attributed to the prestressing force of the steel strand, the effect of the NSM post-tensioned CFRP strengthening system decreased. The difference in the strengthening ratio of the initial crack loads in PNSM-C40-P140 and PNSM-C40-P280 using the normal concrete (40 MPa) was found to be below 14%. The test unit using the normal concrete was to endure more compressive stress, making it possible to maintain a strengthening ratio higher than 30%, even after introducing the NSM post-tensioned CFRP strengthening system and applying a high prestressing force (280 kN). In all cases, as the compressive strength and the prestressing force increased, the strengthening ratio of the yield and ultimate loads increased by up to 31.1%.

Fig. 7 shows the strain results under the compressive strength and the prestressing force of the steel strand. Fig. 7a shows the strain of the CFRP bar measured in the NSM post-tensioned CFRP strengthening system, which reached 7,850 $\mu\varepsilon$, whereas the theoretical strain of the CFRP bar under the ultimate load was 18,680 $\mu\varepsilon$. Therefore, the CFRP bar underwent brittle destruction when a strain of over 10,830 $\mu\varepsilon$ was applied. The strains of the CFRP bar for PNSM-C40-P140 and PNSM-C40-P280 were 6,196 $\mu\varepsilon$ and 6,940 $\mu\varepsilon$, respectively. The strains of the CFRP bar for PNSM-C20-P140 and PNSM-C20-P280 for a compressive strength of 20 MPa were 7,223 $\mu\varepsilon$ and 6,057 $\mu\varepsilon$, respectively. However, the PSC beam with the NSM post-tensioned CFRP strengthening system did not exhibit brittle destruction of the CFRP bar in all cases considering the steel strands shared the load. Moreover, the experiments for all test units were discontinued without attaining the brittle destruction of the CFRP bar considering the concrete rush caused the load to decrease. Fig. 7b shows the strain of the steel reinforcement measured in the PSC beam to which the NSM post-tensioned CFRP strengthening system was applied. The compressive strength and the prestressing force of the steel strand were found to be high in PNSM-C40-P280,

Table 4 Strengthening ratio with and without the prestressing load of the CFRP bar

Test unit	Initial cracking		Yielding		Ultimate	
	Load (kN)	Strengthening ratio (%)	Load (kN)	Strengthening ratio (%)	Load (kN)	Strengthening ratio (%)
NS-C20-P140	46.6	–	180.4	–	227.6	–
NSM-C20-P140	42.6	8.6	187.8	4.1	248.0	9.0
PNSM-C20-P140	67.5	44.8	214.8	19.1	278.0	22.1

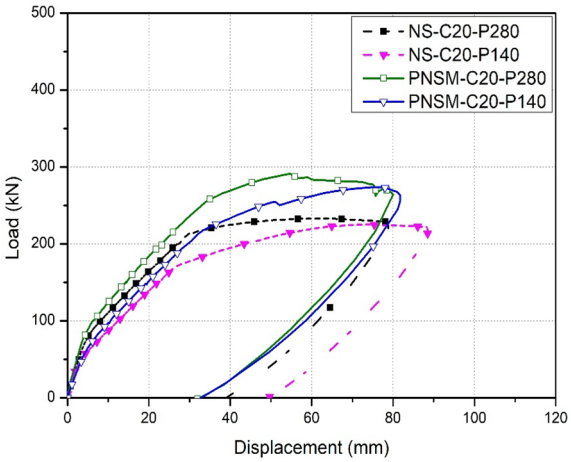

(a) Concrete compressive strength = 20 MPa

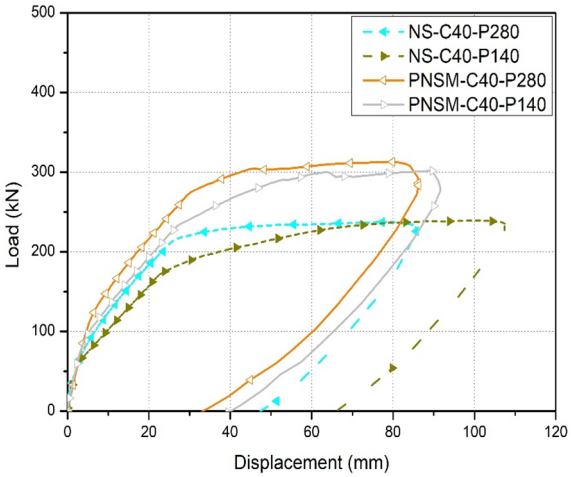

(b) Concrete compressive strength = 40 MPa

Fig. 6 Displacement results under the compressive strength and prestressing of the steel strand

thereby indicating that the yielding of the steel reinforcement occurred at the highest load (286.9 kN). Because PNSM-C40-P140 (232.0 kN) exhibited the compressive strength, yield load was higher than that of PNSM-C20-P140 (214.8 kN). However, the prestressing force of the steel strand was lower than that of PNSM-C20-P280 (255.8 kN). Therefore, the PSC beam to which the NSM post-tensioned CFRP strengthening system was applied exhibited an increase in compressive strength and the prestressing force, which increased the yield load of the steel reinforcement.

5 Finite-Element Analysis

A three-dimensional (3D) FE model was developed to analyze the flexural strengthening efficiency of the strengthened PSC beam with the NSM post-tensioned CFRP strengthening system. The results of the FEA were compared to that of the experiments.

Various functions and finite elements of ABAQUS (Dassault Systèmes, France) (2021) were utilized for the analysis. Fig. 8 shows the components of FE model and the boundary conditions in detail. The concrete was modeled with the general-purpose linear brick element with reduced integration (C3D8R). A Euler–Bernoulli beam element (B33) was used for modeling of steel reinforcement under resisting tensile force. The shear behavior acts as a major variable in the anchorage device because of the prestressing force of the CFRP bar. Therefore, a Timoshenko beam element (B31) was used to model under shear force. ABAQUS (2021) presented a truss element when implementing a structure to introduce the prestress. Therefore, this study utilized a two-node linear truss element (T3D2) to apply the steel strand and CFRP bar. Poisson's ratio and elasticity E_c of the concrete were set to 0.167 and $4,700\sqrt{f_c}$ MPa, respectively (American Concrete Institute, 2019). f_c is the compressive strength of the concrete measured in the experiment. The elasticity (200,000 MPa) and Poisson's ratio (0.3) of the steel

Table 5 Strengthening ratio according to the compressive strength and prestressing load of the steel strand

Test unit	Initial cracking		Yielding		Ultimate	
	Load (kN)	Strengthening ratio (%)	Load (kN)	Strengthening ratio (%)	Load (kN)	Strengthening ratio (%)
NS-C20-P140	46.6	–	180.4	–	227.6	–
PNSM-C20-P140	67.5	44.8	214.8	19.1	278.0	22.1
NS-C20-P280	77.5	–	209.2	–	233.2	–
PNSM-C20-P280	86.3	11.4	255.8	22.3	290.0	24.4
NS-C40-P140	63.7	–	188.5	–	239.3	–
PNSM-C40-P140	92.3	44.9	232.0	23.1	300.0	25.4
NS-C40-P280	93.5	–	218.8	–	237.6	–
PNSM-C40-P280	122.6	31.1	286.9	31.1	311.0	30.9

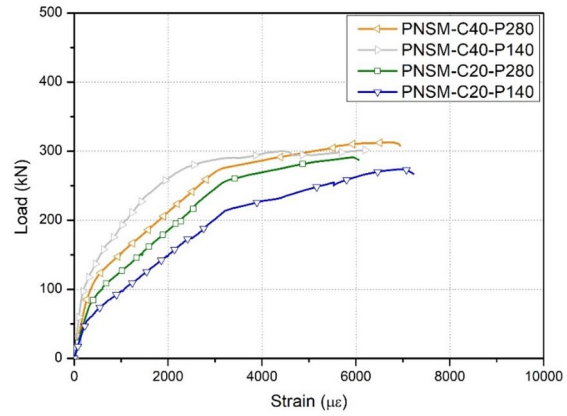

(a) CFRP bar

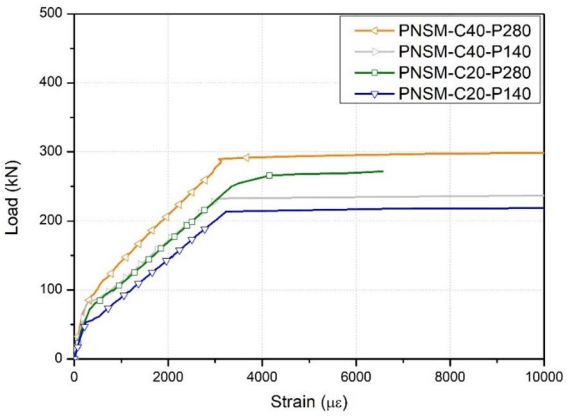

(b) Steel reinforcement

Fig. 7 Strain results according to compressive strength and prestressing of steel strand

reinforcement, steel strand, and anchorage device were defined. Also, the elasticity (167,000 MPa) and Poisson's ratio (0.27) of the CFRP bar were defined, respectively. The loads were classified during the initial and loading steps. In the initial step, an initial stress of 1,283 MPa (42% of tensile strength) was applied to the prestressing for the CFRP bar. Previous studies (Cho et al., 2022, 2024; Lee et al., 2017a, 2017b, 2019, 2024) examined the slip and friction behavior of CFRP experimentally and analytically. The CFRP anchorage system employed does not induce slip or friction until the tensile failure of CFRP. Consequently, the analysis model was conducted under the assumption that no prestressing loss occurred. The boundary conditions are as shown in Fig. 8b. The implicit FEA was performed by applying a vertical load to the PSC beam using the Newton–Raphson method in the loading step. For the vertical load, the initial increment (0.005), minimum increment (1.0×10^{-5}), and maximum increment (0.01) were set, respectively.

Considering the plastic regime of each material of the material nonlinearity, the modeling method within the ABAQUS (2021) was used. The concrete damaged plasticity (CDP) material model was introduced to analyze the plastic behavior of concrete (ABAQUS, 2021). The nonlinear behavior of steel reinforcement, anchorage device, steel strand, and CFRP bar was implemented using the plastic material model in ABAQUS (2021).

Herein, three interfaces were considered during the modeling of the NSM post-tensioned CFRP strengthening system. The first interface was formed between the concrete and the epoxy. During the experiment, no contact surface cracks were observed between the concrete and the epoxy. Therefore, the first interface was implemented to be bonded tightly. The next was the interface between the CFRP and the epoxy. The CFRP was embedded into the epoxy. The embedded element technique (EET) implemented the element restricted in host elements (ABAQUS, 2021). Moreover, this technique was used to implement the steel reinforcement and steel strands in the concrete. Therefore, the interface between the CFRP and the epoxy was defined as the EET. The final interface was formed at the anchorage device that fixed CFRP. In the experiment, slips due to destruction were not observed in the final interface. Therefore, the final interface was implemented as the rigid link.

Fig. 9 compares the load–deformation relationship between the FEA and the experiment. This study aimed to perform FEA based on PNSM-C40-P280, which is the ideal state. The initial concrete crack, steel yield, and ultimate load obtained during FEA were analyzed and compared to the experimental results. The initial concrete crack load was 122.6 kN and 120.0 kN in the experiment and FEA, respectively, with a difference of approximately 2.1%, as shown in Fig. 9a. The error rate of the steel yield load of the experiment (286.9 kN) and FEA (290.0 kN) was found to be below 1.1%. The ultimate load based on the experimental and FEA results was 311.0 kN and 317.0 kN, respectively. The difference ratio of the ultimate load between the experimental and FEA results was smaller than 2%. Fig. 9b shows the strain generated in the CFRP bar, which was found to be 6,940 $\mu\varepsilon$ and 7,525 $\mu\varepsilon$, in the experiment and FEA, respectively, with a difference ratio of was approximately 8%. It is predicted that this value was obtained, because the connection between the CFRP bar and PSC beam was stiffer in the FEA than in the experiment. The suggested FE model predicted the error rates of initial concrete crack, steel yield, and the ultimate load to be less than 3%, and implemented a similar CFRP bar behavior to the experiments. Therefore, in this study, the flexural behavior of the NSM post-tensioned CFRP strengthening system under PSC beam could be predicted using the suggested FE model.

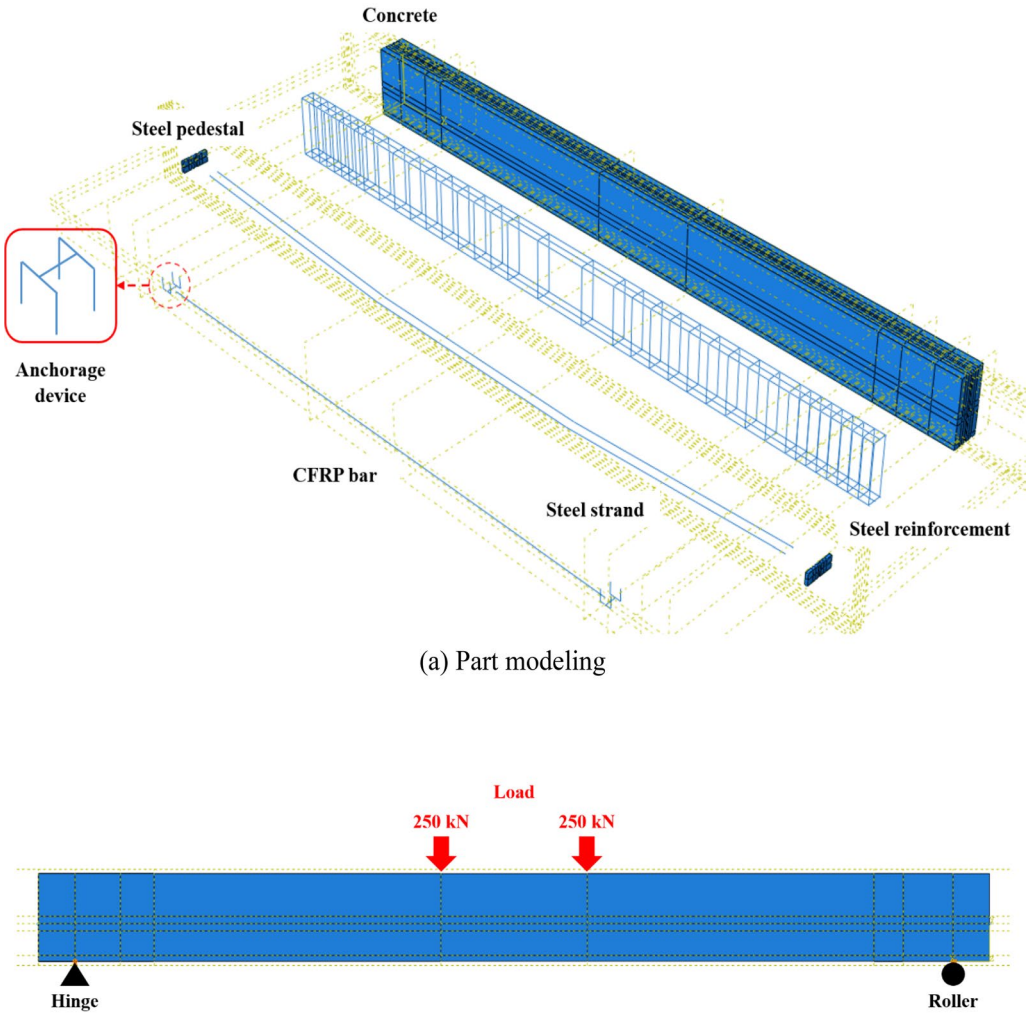

Fig. 8 Finite-element model

The crack pattern on the concrete surface and stress distribution of PNSM-C40-P280 were analyzed using the suggested FE model. Fig. 10 shows the crack pattern of PNSM-C40-P280 observed from the experiments. In PNSM-C40-P280, vertical cracks at the bottom occurred owing to the ultimate load. Simultaneously, in the upper part of PNSM-C40-P280, the compressive force exceeded the compressive strength, resulting in a concrete crush. This can be attributed to the ultimate load, which indicates the occurrence of a tensile and compression failure mode. Fig. 11 shows the maximum principal stress distribution exhibited by the load level in the suggested FE model. At a load of 150 kN, a region at the bottom of the suggested FE model exceeded the tensile limit stress (4 MPa). The region exceeding the bottom tensile limit stress spread when the load was between 200 and 250 kN. At the ultimate load (317 kN), the suggested FE model exhibited stress that exceeded the compression limit stress (40 MPa) in the upper part, resulting in a concrete crush. Additionally, the region exceeding the tensile limit stress at the bottom spread to the upper part. Therefore, at the bottom of the suggested FE model, the region exceeding the tensile limit stress increased as the load increased. However, at the top, the region exceeding the compression limit stress was generated owing to the ultimate load. Therefore, the maximum principal stress distribution in the FEA exhibited a similar behavior to the crack in the experiment. As a result, the suggested FE model predicted the failure mode of the NSM post-tensioned CFRP strengthening system under PSC beam.

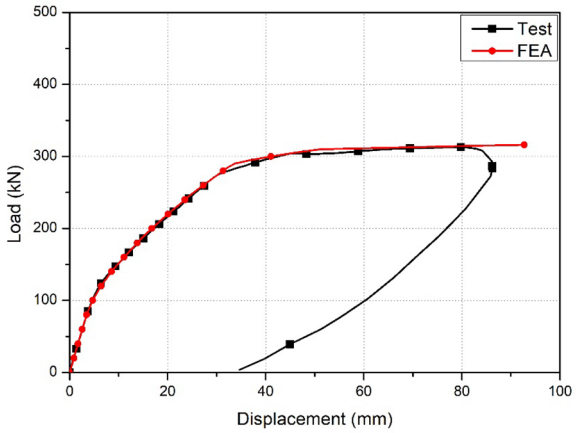

(a) Displacement

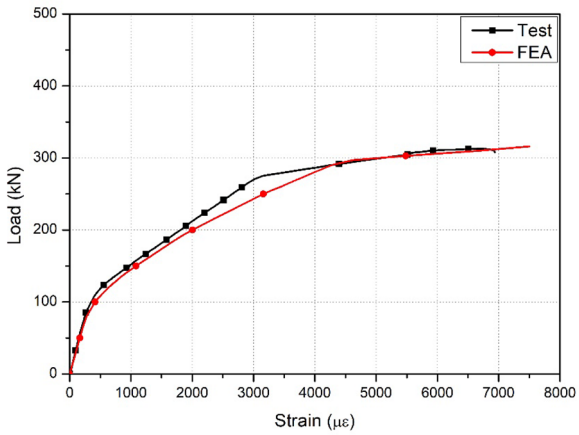

(b) Strain of CFRP bar

Fig. 9 Load–deformation comparison between thefinite-element analysis and experimental results

6 Parametric Study Using The Suggested Finite-Element Model

Table 6 presents the FEA parameters. A parametric study was conducted to analyze the results obtained using different steel reinforcement ratios and compressive strengths that were not identified in the experiments. Steel reinforcement ratios of 0.0024, 0.0038, and 0.0055 and compressive strengths of 30 MPa, 40 MPa, and 50 MPa were used. In this study, the different cases of steel reinforcement ratios and compressive strengths were divided based on that of PNSM-C40-D16 to analyze the flexural behavior of the FE model. Fig. 12 shows the displacement results of the parametric study according to the steel reinforcement ratio and compressive strength of the concrete. For the initial crack load, the compressive strength and prestressing force were dominant, indicating that the effect of the steel reinforcement ratio was small. Therefore, this study focused on analyzing the steel yield load and ultimate load with varying steel reinforcement ratios. When the steel reinforcement ratio was higher than that of PNSM-C40-D16 (PNSM-C40-D19), the steel loading and ultimate load increased by 21.4% and 21.5%, respectively. Conversely, when the steel reinforcement ratio was lower (PNSM-C40-D13), the steel yield and ultimate load decreased by 16.9% and 16.4%, respectively (Fig. 12a). As shown in Fig. 12b, PNSM-C50-D16 exhibited a larger compressive strength compared to PNSM-C40-D16, and hence, the initial crack load, steel yield, and ultimate load increased by 16.7%, 8.6%, and 10.1%, respectively. In PNSM-C30-D16, the compressive strength was lower, due to which the initial crack load, steel yield load, and ultimate load decreased by 20.8%, 10.3%, and 9.8%, respectively, compared to those of PNSM-C40-D16.

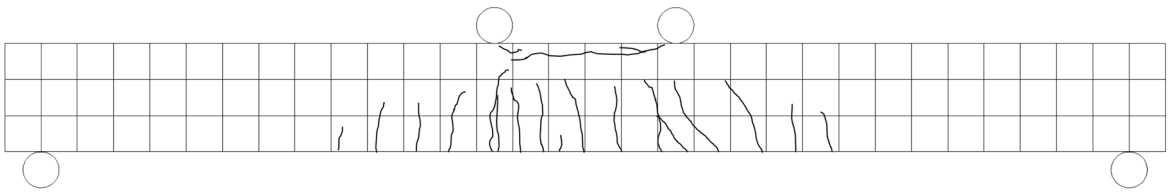

(a) Crack at 317 kN (ultimate load)

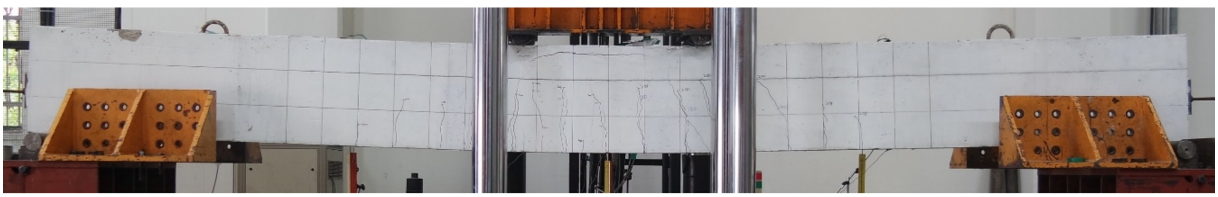

(b) Crack shape

Fig. 10 Final crack pattern of the test (PNSM-C40-P280)

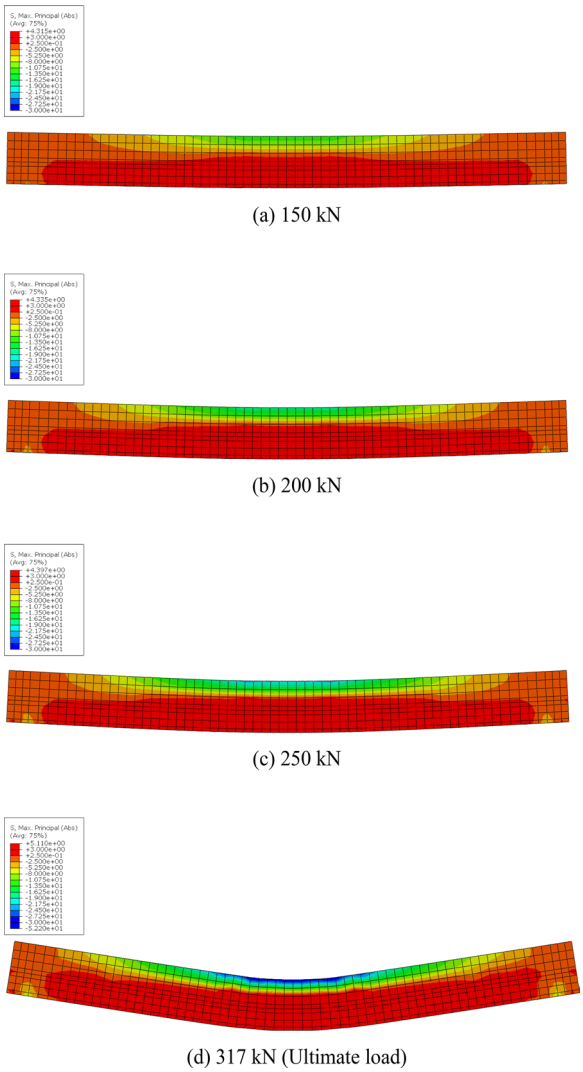

(a) 150 kN

(b) 200 kN

(c) 250 kN

(d) 317 kN (Ultimate load)

Fig. 11 Stress distribution of thefinite-element model

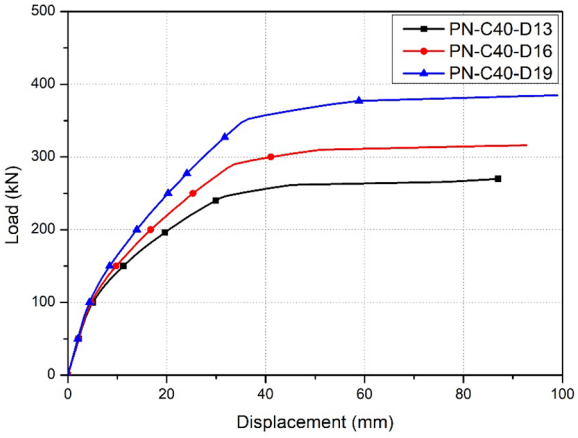

(a) Steel reinforcement ratio

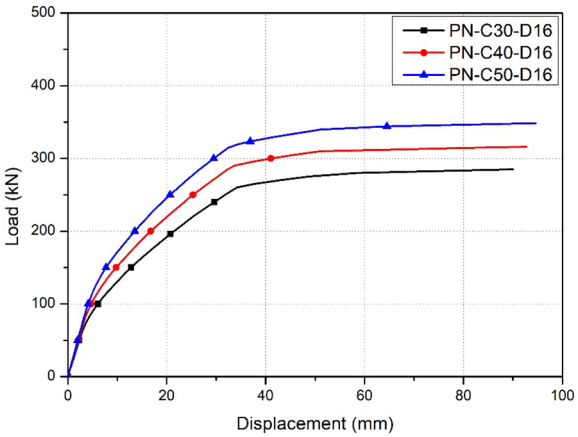

(b) Compressive strength of concrete

Fig. 12 Displacement results of the parametric study

Table 6 Parameters of the finite element analysis

Parameter name	Compressive strength of the concrete (MPa)	Steel reinforcement ratio
PNSM-C40-D13	40	0.0024 (380 mm^2, 3-D13)
PNSM-C40-D16		0.0038 (597 mm^2, 3-D16)
PNSM-C40-D19		0.0055 (861 mm^2, 3-D19)
PNSM-C30-D16	30	0.0038 (597 mm^2, 3-D16)
PNSM-C50-D16	50	0.0038 (597 mm^2, 3-D16)

Fig. 13 shows the ultimate load trend according to the parameters. In terms of the strengthened PSC beam with the NSM post-tensioned CFRP strengthening system, the ultimate load increased close to the line as the steel reinforcement ratio increased (Fig. 13a). Fig. 13b shows the ultimate load trend according to the compressive strength. In the NSM post-tensioned CFRP strengthening system strengthened PSC beam, the ultimate load improved at a constant rate as the steel reinforcement ratio increased. Therefore, these parameters should be the main design factors when using the NSM post-tensioned CFRP strengthening system, considering the strengthening effect of the NSM post-tensioned CFRP strengthening system improves according to the steel reinforcement ratio and compressive strength.

7 Conclusion

In this study, four-point loading experiments were conducted to analyze the flexural strengthening effect of the NSM post-tensioned CFRP strengthening system under PSC beam depending on the strengthening method and

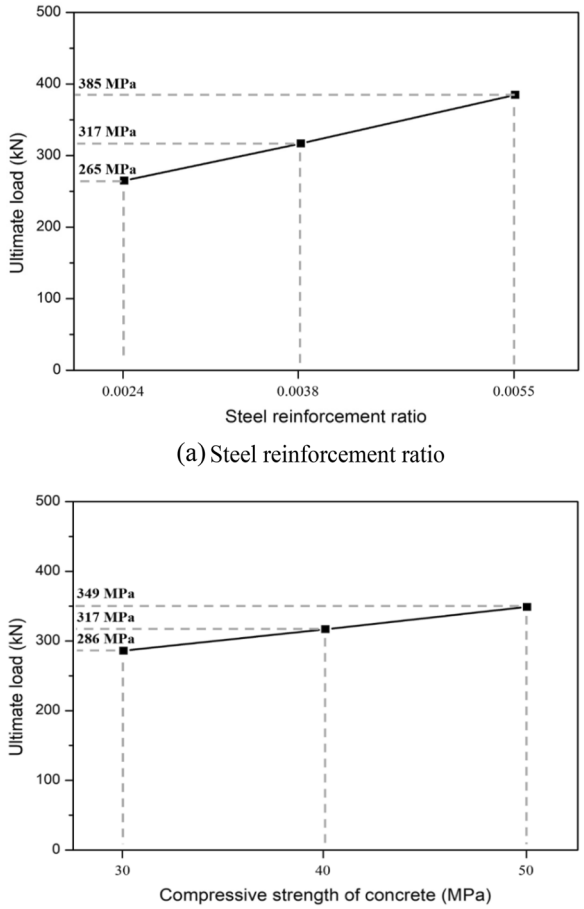

Fig. 13 Ultimate load trend according to the experiment parameters

material properties. Furthermore, a 3D finite-element nonlinear analysis was conducted to compare the flexural behavior of the strengthened PSC beam through experiments and FEA. Finally, a parametric study was performed. The results of the different strengthening methods and material properties of the PSC beam are as follows:

1. Compared to the PSC reference beam, the ultimate load of the NSM with post-tensioned and non-post-tensioned CFRPs strengthening system under PSC beam increased by up to 22.1% and 9.0%, respectively. Moreover, the initial crack load of the NSM post-tensioned CFRP strengthening system strengthened PSC beam increased by 44.8%, whereas that of the PSC beam using the NSM non-post-tensioned CFRP strengthening system increased by less than 9%, compared to those of the PSC reference beam. Therefore, the NSM post-tensioned CFRP strengthening system was superior to the NSM non-post-tensioned CFRP strengthening system.
2. The ultimate load of the strengthened PSC beam with the NSM post-tensioned CFRP strengthening system using normal concrete (40 MPa) and deteriorated concrete (20 MPa) increased by up to 30.9% and 24.4%, respectively. The endurable stress in the concrete increased in the NSM post-tensioned CFRP strengthening system when normal concrete was used owing to the high compressive strength, which resulted in an improved flexural strengthening effect.
3. Compared to the PSC reference beam, the ultimate load of the appropriate prestressing force of the steel strand (280 kN) increased by up to 30.9%, and that of half the appropriate prestressing force of the steel strand (140 kN) increased by up to 25.4%. Therefore, when the prestress loss is low, the initial crack load of the PSC beam increases, which in turn increases the flexural strengthening effect of the NSM post-tensioned CFRP strengthening system. In addition, the NSM post-tensioned CFRP strengthening system reinforced the structural performance of PSC structures due to the high strengthening effect even if the prestressing force decreases according to the aging of steel strands.
4. The NSM post-tensioned CFRP strengthening system with normal concrete (40 MPa) maintained a strengthening ratio of over 30% at the initial crack load, even when the appropriate prestressing force of the steel strand (280 kN) was used. However, the strengthening ratio of the initial crack load of the NSM post-tensioned CFRP strengthening system with deteriorated concrete (20 MPa) rapidly decreased from 44.8% to 11.4% as the prestressing force of the steel strand increased. Because the tensile limit stress of the NSM post-tensioned CFRP strengthening system with deteriorated concrete is low, the initial crack generated more rapidly. Therefore, the resistance of the NSM post-tensioned CFRP strengthening system against the initial crack decreased as the concrete aged.
5. The difference ratio of the design compared to experiment decreased as the compressive strength increased. The difference ratio of the initial crack load and ultimate load between the design and test was found to be lower than 3% when the compressive strength was 40 MPa. Conversely, when the compressive strength was 20 MPa, the damage to the anchorage device increased, which increased the difference ratio of the design compared to experiment by up to 25.5%. Therefore, the NSM post-tensioned CFRP strengthening system exhibits a high difference ratio

of the design compared to experimental values under deteriorated concrete.

6. The suggested FE model predicted the flexural behavior and failure mode of the experiment. Furthermore, the suggested FE model implemented the initial stiffness that appeared in the experiment and predicted the initial concrete crack load, steel yield load, and ultimate load with an error rate of less than 3%. Furthermore, the stress distribution of the suggested FE model was similar to that of the test unit. Therefore, the suggested FE model can predict the flexural behavior and failure mode of the NSM post-tensioned CFRP strengthening system under PSC beam.
7. According to the results of the parametric study, the ultimate load of the suggested FE model increased close to linearity as the steel reinforcement ratio and the compressive strength increased. Therefore, considering the flexural strengthening effect increases according to the parameters of the PSC structure in the NSM post-tensioned CFRP strengthening system, the material properties should be considered as the main factors.
8. In this study, the NSM post-tensioned CFRP strengthening system has a high strengthening effect on deteriorated PSC structures. There was a difference between design and experiments of the NSM post-tensioned CFRP strengthening system under deteriorated PSC beam, so it is necessary to supplement the design method in the future. However, the NSM post-tensioned CFRP strengthening system has excellent strengthening effect even in severely deteriorated PSC structures. Therefore, the NSM post-tensioned CFRP strengthening system is expected to be an effective way to solve the problem of deteriorated low-strength PSC structures.

Abbreviations

PSC	Prestressed concrete
CFRP	Carbon fiber-reinforced polymer
FRP	Fiber-reinforced polymer
RC	Reinforced concrete
NSM	Near-surface mounted
UTM	Universal testing machine

Acknowledgements

No applicable.

Author contributions

SC: Writing—original draft preparation; WC: writing and editing, and project administration; WJ: data curation and formal analysis; SP: investigation and conceptualization; HL: formal analysis, and writing and editing;

Funding

This research was supported by a grant(17SCIP-B128496-01) from Smart Civil Infrastructure Research Program funded by Ministry of Land, Infrastructure and Transport of Korean government and the Basic Science Research Program through the National Research Foundation of Korea (NRF) funded by the Ministry of Education (2020R1C1C1005448, 2021R1A2C1011517).

Availability of data and materials

The data and materials are included in the manuscript.

Declarations

Ethics approval and consent to participate

Not applicable.

Consent for publication

Not applicable.

Competing interests

The authors declare that they have no competing interests.

Received: 28 June 2023 Accepted: 5 May 2024
Published online: 03 September 2024

References

Abaqus, A. (2021). *Dassault systems simulia corp; ABAQUS: Providence* (p. 2021). RI.

Ahmed, S., Sharaky, I. A., Ibrahim, Y. E., & Abdo, A. (2023). Flexural response of GFRP RC beams strengthened with side and bottom NSM GFRP bars. *Case Studies in Construction Materials, 18*, e01858. https://doi.org/10.1016/j.cscm.2023.e01858

Allawi, A. A. (2017). Behavior of strengthened composite prestressed concrete girders under static and repeated loading. *Advances in Civil Engineering*. https://doi.org/10.1155/217/3619545

Asamoto, S., Kato, K., & Maki, T. (2014). Effect of creep induction at an early age on subsequent prestress loss and structural response of prestressed concrete beam. *Construction and Building Materials, 70*, 158–164. https://doi.org/10.1016/j.conbuildmat.2014.07.028

Badawi, M., & Soudki, K. (2009). Flexural strengthening of RC beams with prestressed NSM CFRP rods–experimental and analytical investigation. *Construction and Building Materials, 23*(10), 3292–3300. https://doi.org/10.1016/j.conbuildmat.2009.03.005

Barham, W. S., Obaidat, Y. T., & Abdelrahman, B. N. (2021). Experimental study on bond behavior between heat-damaged recycled asphalt pavement concrete and NSM-CFRP strips. *Case Studies in Construction Materials, 14*, e00543. https://doi.org/10.1016/j.cscm.2021

Building code requirements for structural concrete (ACI 318–19). 2019 Farmington Hills, MI: American Concrete Institute.

Caro, L. A., Martí-Vargas, J. R., & Serna, P. (2013). Prestress losses evaluation in prestressed concrete prismatic specimens. *Engineering Structures, 48*, 704–715. https://doi.org/10.1016/j.engstruct.2012.11.038

Cho, S., Chung, W., Jung, W. T., Park, J. S., & Lee, H. (2024). Assessment of shear capacity in NSM prestressed FRP strengthening with anchorage conditions. *Case Studies in Construction Materials, 20*, e02743. https://doi.org/10.1016/j.cscm.2023.e02743

Cho, S., Lee, H., & Chung, W. (2022). Strengthening effect of prestressed near-surface mounted CFRP bar system according to material properties of aged reinforced concrete beams. *Composite Structures, 282*, 115121.

Choi, H. T., West, J. S., & Soudki, K. A. (2011). Effect of partial unbonding on prestressed near-surface-mounted CFRP-strengthened concrete T-beams. *Journal of Composites for Construction, 15*(1), 93–102. https://doi.org/10.1061/(ASCE)CC.1943-5614.0000149

Collins, M. P., & Mitchell, D. (1997). Prestressed concrete structures. Response Publications.

Correia, L., Teixeira, T., Michels, J., Almeida, J. A., & Sena-Cruz, J. (2015). Flexural behaviour of RC slabs strengthened with prestressed CFRP strips using different anchorage systems. *Composites Part b: Engineering, 81*, 158–170. https://doi.org/10.1016/j.compositesb.2015.07.011

Design and construction of building components with fibre-reinforced polymers. Canadian Standards Association: Toronto

El-Hacha, R., & Gaafar, M. (2011). Flexural strengthening of reinforced concrete beams using prestressed near-surface mounted CFRP bars. *PCI Journal*. https://doi.org/10.15554/pcij.09012011.134.151

Esmaeeli, E., & He, Y. (2021). Cast-in-situ vs prefabricated solution based on NSM-CFRP reinforced SHCC for seismic retrofitting of severely damaged substandard RC beam-column joints. *Journal of Building Engineering, 43*, 103132.

Guide for the design and construction of structural concrete reinforced with FRP bars (ACI 440.1R-15). 2015 Farmington Hills, MI: American Concrete Institute.

Haddad, R. H., & Yaghmour, E. M. (2020). Side NSM CFRP strips with different profiles for strengthening reinforced concrete beams. *Journal of Building Engineering, 32*, 101772.

Herrmann, A. W. (2013, May). Asce 2013 report card for america's infrastructure. In *IABSE symposium report* 99, 33, 9–10). International Association for Bridge and Structural Engineering.

Hong, K., Lee, S., Yeon, Y., & Jung, K. (2018). Flexural response of reinforced concrete beams strengthened with near-surface-mounted Fe-based shape-memory alloy strips. *International Journal of Concrete Structures and Materials, 12*(1), 1–13.

Hong, S., & Park, S. K. (2016). Effect of prestress and transverse grooves on reinforced concrete beams prestressed with near-surface-mounted carbon fiber-reinforced polymer plates. *Composites Part b: Engineering, 91*, 640–650. https://doi.org/10.1016/j.compositesb.2016.01.018

Jafari, A., Oskouei, A. V., Bazli, M., & Ghahri, R. (2018). Effect of the FRP sheet's arrays and NSM FRP bars on in-plane behavior of URM walls. *Journal of Building Engineering, 20*, 679–695. https://doi.org/10.1016/j.jobe.2018.09.018

JSCE Concrete Committee. (2007). Concrete Using Continuous Fiber Reinforcing Materials (CFRM). In J. P. N. Tokyo (Ed.), *Standard specifications for concrete structures-Materials and construction* (pp. 289–298). Japan Society of Civil Engineers.

Kara, I. F., Ashour, A. F., & Köroğlu, M. A. (2016). Flexural performance of reinforced concrete beams strengthened with prestressed near-surface-mounted FRP reinforcements. *Composites Part b: Engineering, 91*, 371–383. https://doi.org/10.1016/j.compositesb.2016.01.023

Kim, S. H., Park, J. S., Jung, W. T., Kim, T. K., & Park, H. B. (2021). Experimental study on strengthening effect analysis of a deteriorated bridge using external prestressing method. *Applied Sciences, 11*(6), 2478. https://doi.org/10.3390/app11062478

Kwon, S. J., Yang, K. H., & Mun, J. H. (2018). Flexural tests on externally post-tensioned lightweight concrete beams. *Engineering Structures, 164*, 128–140.

Lee, H., Jeong, S., & Chung, W. (2024). Enhancing bond performance: Carbon fiber reinforced polymer bar interaction with multi-walled carbon nanotubes cementitious composites in chloride-exposed conditions. *Construction and Building Materials, 412*, 134763.

Lee, H., Jung, W. T., & Chung, W. (2017a). Flexural strengthening of reinforced concrete beams with pre-stressed near surface mounted CFRP systems. *Composite Structures, 163*, 1–12. https://doi.org/10.1016/j.compstruct.2016.12.044

Lee, H., Jung, W. T., & Chung, W. (2017b). Post-tension near-surface-mounted strengthening systems of full-scale PSC girders. *Construction and Building Materials, 151*, 71–82. https://doi.org/10.1016/j.conbuildmat.2017.06.070

Lee, H., Jung, W. T., & Chung, W. (2018). Field test of an old RC bridge before and after NSM strengthening. *Composite Structures, 202*, 793–801. https://doi.org/10.1016/j.compstruct.2018.04.024

Lee, H., Jung, W. T., & Chung, W. (2019). Post-tension near-surface mounted strengthening system for reinforced concrete beams with changes in concrete condition. *Composites Part b: Engineering, 161*, 514–529. https://doi.org/10.1016/j.compositesb.2018.12.149

Mansour, M., & El-Maaddawy, T. (2021). Testing and modeling of deep beams strengthened with NSM-CFRP reinforcement around cutouts. *Case Studies in Construction Materials, 15*, e00670. https://doi.org/10.1016/j.cscm.2021.e00670

Nordin, H., & Täljsten, B. (2006). Concrete beams strengthened with prestressed near surface mounted CFRP. *Journal of Composites for Construction, 10*(1), 60–68. https://doi.org/10.1061/(asce)1090-0268(2006)10:1(60)

Noroozieh, E., & Mansouri, A. (2019). Lateral strength and ductility of reinforced concrete columns strengthened with NSM FRP rebars and FRP jacket. *International Journal of Advanced Structural Engineering, 11*(2), 195–209.

Páez, P. M., & Sensale, B. (2018). Improved prediction of long-term prestress loss in unbonded prestressed concrete members. *Engineering Structures, 174*, 111–125. https://doi.org/10.1016/j.engstruct.2018.07.038

Panahi, M., Zareei, S. A., & Izadi, A. (2021). Flexural strengthening of reinforced concrete beams through externally bonded FRP sheets and near surface mounted FRP bars. *Case Studies in Construction Materials, 15*, e00601. https://doi.org/10.1016/j.cscm.2021.e00601

Peng, H., Zhang, J., Cai, C. S., & Liu, Y. (2014). An experimental study on reinforced concrete beams strengthened with prestressed near surface mounted CFRP strips. *Engineering Structures, 79*, 222–233. https://doi.org/10.1016/j.engstruct.2014.08.007

Pisani, M. A. (2018). Behaviour under long-term loading of externally prestressed concrete beams. *Engineering Structures, 160*, 24–33.

Prestressing concrete structures with FRP tendons (ACI 440.4 R-04). 2004 Farmington Hills, MI: American Concrete Institute.

Salman, W. D., & Mansor, A. A. (2021). Fibrous geopolymer paste composites for near-surface-mounted strengthening of reinforced concrete beams in flexure. *Case Studies in Construction Materials, 14*, e00529.

Seo, S. Y., Choi, K. B., Kwon, Y. S., & Lee, K. S. (2016). Flexural strength of RC beam strengthened by partially de-bonded near surface-mounted FRP strip. *International Journal of Concrete Structures and Materials, 10*(2), 149–161.

Sokairge, H., Elgabbas, F., & Elshafie, H. (2022). Structural behavior of RC beams strengthened with prestressed near surface mounted technique using basalt FRP bars. *Engineering Structures, 250*, 113489.

State-of-the-art report on partially prestressed concrete (ACI 423.5R-99). 1999 Farmington Hills, MI: American Concrete Institute.

Stewart, M. G., & Rosowsky, D. V. (1998). Time-dependent reliability of deteriorating reinforced concrete bridge decks. *Structural Safety, 20*(1), 91–109.

Vollmer, M., Bauer, A., Frenck, J. M., Krooß, P., Wetzel, A., Middendorf, B., & Niendorf, T. (2021). Novel prestressing applications in civil engineering structures enabled by FeMnAlNi shape memory alloys. *Engineering Structures, 241*, 112430. https://doi.org/10.1016/j.engstruct.2021.112430

Wongkeo, W., Thongsanitgarn, P., Ngamjarurojana, A., & Chaipanich, A. (2014). Compressive strength and chloride resistance of self-compacting concrete containing high level fly ash and silica fume. *Materials & Design, 64*, 261–269. https://doi.org/10.1016/j.matdes.2014.07.042

Wu, G., Dong, Z. Q., Wu, Z. S., & Zhang, L. W. (2014). Performance and parametric analysis of flexural strengthening for RC beams with NSM-CFRP bars. *Journal of Composites for Construction, 18*(4), 04013051. https://doi.org/10.1061/(asce)cc.1943-5614.0000451

Xiang, T., & Zhao, R. (2007). Reliability evaluation of chloride diffusion in fatigue damaged concrete. *Engineering Structures, 29*(7), 1539–1547. https://doi.org/10.1016/j.engstruct.2006.09.002

Ye, C., Butler, L. J., Elshafie, M. Z., & Middleton, C. R. (2020). Evaluating prestress losses in a prestressed concrete girder railway bridge using distributed and discrete fibre optic sensors. *Construction and Building Materials, 247*, 118518.

Yildirim, K., & Sümer, M. (2013). Effects of sodium chloride and magnesium sulfate concentration on the durability of cement mortar with and without fly ash. *Composites Part b: Engineering, 52*, 56–61. https://doi.org/10.1016/j.compositesb.2013.03.040

You, R., & Kaewunruen, S. (2019). Evaluation of remaining fatigue life of concrete sleeper based on field loading conditions. *Engineering Failure Analysis, 105*, 70–86. https://doi.org/10.1016/j.engfailanal.2019.06.086

Yu, X., Xing, G., & Chang, Z. (2020). Flexural behavior of reinforced concrete beams strengthened with near-surface mounted 7075 aluminum alloy bars. *Journal of Building Engineering, 31*, 101393.

Zhao, G., Li, J., Shi, M., Cui, J., & Xie, F. (2020). Degradation of cast-in-situ concrete subjected to sulphate-chloride combined attack. *Construction and Building Materials, 241*, 117995.

Publisher's Note

Sanghyeon Cho is Doctor in Department of Civil Engineering, College of Engineering at Kyung Hee University, Gyeonggi, Republic of Korea.

Wonseok Chung is Professor in Department of Civil Engineering, College of Engineering at Kyung Hee University, Gyeonggi, Republic of Korea.

Woo-tai Jung is Research Fellow in Advanced Composites Research Center, Korea Institute of Civil Engineering and Building Technology, Gyeonggi, Republic of Korea.

Jong-sup Park is Research Fellow in Advanced Composites Research Center, Korea Institute of Civil Engineering and Building Technology, Gyeonggi, Republic of Korea.

Heeyoung Lee is Associate Professor in Department of Civil Engineering at Chosun University, Gwangju, Republic of Korea.